High-Power THz Generation, THz Nonlinear Optics, and THz Nonlinear Spectroscopy

János Hebling, Ka-Lo Yeh, Matthias C. Hoffmann, and Keith A. Nelson

(Invited Paper)

***Abstract*—It is now possible to generate terahertz (THz) pulses with sufficient energy and field amplitude to enable versatile applications in THz nonlinear optics and spectroscopy. In addition, THz waveform shaping at high intensities promises wide ranging new capabilities in THz coherent control. We review recent progress in generation of high-power THz phonon–polariton waves in lithium niobate that can be coupled into free space THz radiation. A "polaritonics" toolset for control and processing of the THz waves is also reviewed briefly. Recent demonstrations of THz nonlinear optics and spectroscopy are then presented.**

***Index Terms*—High-power terahertz sources, lattice anharmonicity, lithium niobate ($LiNbO_3$), nonlinear terahertz optics.**

I. Introduction

TERAHERTZ optics and spectroscopy have advanced technologically and expanded rapidly in their scope of applications in recent years, spurred largely by improvements in methods for generation and characterization of terahertz pulses as short as a single cycle in duration and with spectral content extending from less than 0.1 to 10 THz and beyond [1], [2]. The use of ultrashort terahertz pulses has facilitated terahertz spectroscopy of a wide range of physical, chemical, and biological samples, and has enabled time-resolved measurements in which the terahertz pulse is used to probe dynamical responses to an optical excitation pulse. In almost all cases reported to date, the THz pulses have had rather low energy, field amplitude, and average power. This has slowed the development of nonlinear THz optics and spectroscopy as well as THz signal processing, spectroscopic imaging and screening, and other applications. Free electron lasers can produce THz pulses with energy in the 10–100 μJ range [3]. However, the access of these large-scale facilities is limited, and the THz waveform cannot be arbitrarily shaped. Until recently, the only tabletop source of ultrashort terahertz pulses approaching 1 μJ in energy was a large-aperture photoconductive switch [4] illuminated by ultrashort laser pulses. Its output was used in an early example of ultrafast nonlinear THz spectroscopy involving THz-induced nonlinear electronic responses (including ionization) of Rydberg atoms. However, the spectral peak of the pulses generated by this device was below 0.5 THz, and the high voltage switching involved posed practical challenges and signal/noise limitations that have forestalled further use. Recently, generation of THz responses from plasmas in air and various gases has shown promise for high THz bandwidths and high field amplitudes [5]–[8]. To date, high pulse energies have not been reported.

From the point of view of efficiency, accessibility, and diversity of possible applications, optical rectification of ultrashort laser pulses [9]–[12] is an extremely promising method for generation of THz pulses with high energy, high field amplitude, and high average power. The optical rectification occurs through difference-frequency mixing among the Fourier components that are contained within the spectral bandwidth of the ultrashort optical pulse. Efficient optical rectification requires the group velocity of the ultrashort laser pulse to be equal to the phase velocity of the generated THz radiation [13]. This velocity-matching requirement is conveniently fulfilled in a collinear geometry with ZnTe [9], [14], [15] and GaP [16] as the nonlinear optical materials for pump wavelengths of around 800 nm and 1 μm, respectively. But the nonlinear coefficients of these materials are far smaller than those of some high dielectric, ferroelectric materials including lithium tantalate ($LiTaO_3$) and lithium niobate ($LiNbO_3$). In such materials, THz electromagnetic waves are strongly coupled to highly polar, "soft" optic phonons associated with the ferroelectric phase transitions, yielding mixed phonon–polariton modes [17]. The polarizabilities of these modes give rise to many of the favorable nonlinear optical properties of these materials. For example, the optical rectification in these materials occurs primarily through impulsive stimulated Raman scattering [18], through which the femtosecond optical pulse drives the lattice vibrations and through them the THz phonon–polariton waves.

It was recognized and demonstrated early [19] that the high refractive index values of ferroelectric materials at THz compared to optical frequencies results in a THz response that propagates at a very large (Cherenkov) angle $\Theta_C = \cos^{-1}(\nu_{\mathrm{THz}}^{\mathrm{ph}}/\nu_{\mathrm{vis}}^{\mathrm{gr}})$ relative to the optical beam that produces it, where the ratio of phase and group velocities $\nu_{\mathrm{THz}}^{\mathrm{ph}}/\nu_{\mathrm{vis}}^{\mathrm{gr}}$ is given by that of the group and refractive indexes $n_{\mathrm{vis}}^{\mathrm{gr}}/n_{\mathrm{THz}}$ at visible and THz frequencies, respectively. For example, in stoichiometric $LiNbO_3$ (sLN), the result $n_{\mathrm{vis}}^{\mathrm{gr}}/n_{\mathrm{THz}} = 2.25/4.96 = 0.454$ yields $\Theta_C = 63.0^\circ$. Thus, the THz response propagates mainly laterally away from the optical pump beam. For a round pump spot as used originally [19], the THz response takes the form of a diverging Cherenkov cone

Manuscript received October 16, 2007; revised December 3, 2007. This work was supported in part by the ONR under Grant N00014-06-1-0463 and Grant N00014-06-1-0459 and in part by the NSF Grant CHE-0616939.

J. Hebling is with Massachusetts Institute of Technology, Cambridge, MA 02139 USA, on leave from the University of Pécs, Pécs 7624, Hungary (e-mail: hebling@mit.edu).

K.-L. Yeh, M. C. Hoffmann, and K. A. Nelson are with Massachusetts Institute of Technology, Cambridge, MA 02139 USA (e-mail: kaloyeh@mit.edu; mch@mit.edu; kanelson@mit.edu).

Color versions of one or more of the figures in this paper are available online at http://ieeexplore.ieee.org.

Digital Object Identifier 10.1109/JSTQE.2007.914602

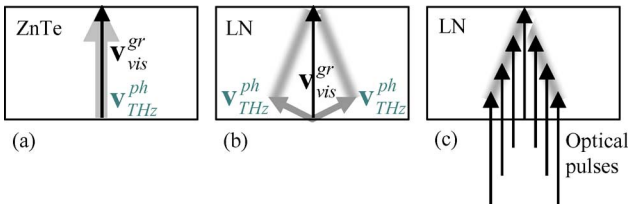

Fig. 1. Top view of THz generation in a nonlinear optical crystal. In all cases, an optical pump pulse propagates from front to back of the crystal (bottom to top in drawings) with wavevector magnitude and direction represented by a black arrow. Terahertz wavevectors are represented by grey arrows, and terahertz single-cycle wavefronts are drawn in grey. (a) Conventional collinear velocity matching, as in ZnTe crystal with 800 nm optical wavelength. The THz field copropagates with the optical pulse that generates it, building up larger THz amplitudes as the two pulses move through the crystal together. (b) THz phonon–polariton generation in the LN crystal. A cylindrically focused optical beam generates THz plane waves that propagate mainly laterally (at the Cherenkov angle) with a modest forward wavevector component relative to the optical beam direction. In this case, the THz field components generated by the optical pulse as it moves through the crystal do not superpose. (c) THz polariton wave generation in the LN crystal as in (b), but with additional, spatially and temporally shifted optical pulses that can be used to monitor the THz wave or to generate additional THz field components that may superpose with it.

that is impractical for most applications. The use of a cylindrically focused optical beam [20], forming a "line" source that moves through the nonlinear optical crystal, results in laterally propagating single-cycle THz plane waves that are far more convenient. Crossed optical beams were also used early to generate optical interference patterns [21], i.e., multiple "line" sources that launched multiple-cycle THz plane waves.

While generation of single-cycle or multiple-cycle THz plane waves in the LN and similar crystals as described earlier is convenient, it does not achieve collinear velocity matching between the optical and the THz waves, and therefore, it does not yield optimal conversion efficiencies or THz pulse energies. The contrast between this situation and the case of collinear velocity matching as in ZnTe or GaP is illustrated in Fig. 1(a) and (b). This might appear to rule out high-dielectric materials for efficient THz generation. However, the laterally propagating THz waves are accessible to additional light, as shown in Fig. 1(c). This has been exploited extensively for THz phonon–polariton imaging [22], [23], as reviewed later. It also enables a kind of velocity matching in which successive optical field components arrive at the nonlinear crystal with increasing temporal and spatial shifts, effectively moving across the crystal at the speed of the polariton wave [24]–[26]. At first, this was achieved through simple means using beamsplitters to generate multiple beams and directing them to arrive at appropriate times and crystal locations. Reconfigurable femtosecond spatio-temporal pulse shaping, and later, nonreconfigurable "echelon" stairstep structures were also used to generate sequences of temporally and spatially shifted pulses that amplified laterally propagating THz phonon–polariton waves [27]. It was shown independently that a grating-lens combination could be used to generate a tilted femtosecond pulse front adjusted so that the projection of the tilted pulse front velocity onto the terahertz propagation direction is equal to the polariton phase velocity [28]–[30]. This approach is far simpler and, because it yields a continuous tilted pulse front rather than a discrete one consisting of separated lines of light, it is far more effective in its use of the crystalline volume for polariton amplification. With a crystal cut for normal incidence transmission of the terahertz wave into free space, single-cycle pulses with about $^1/_4$ μJ energy were generated at 1 kHz repetition rates [31]. As shown later, far higher THz pulse energies have since been achieved at 10 Hz repetition rates, and the results at repetition rates from 10 Hz to 1 MHz hold current records for tabletop THz generation systems. Substantial further improvement is anticipated.

The availability of single-cycle THz pulse energies and correspondingly high THz field amplitudes encourages a broad effort in nonlinear THz spectroscopy of low-frequency electronic and vibrational modes as well as other degrees of freedom including polarization dynamics in ordered and partially disordered ferroelectric crystals, molecular orientational and ionic motion in polar liquids and glasses, hydrogen bonding and intermolecular dynamics in simple and viscoelastic liquids and biological media-–in short, most of the degrees of freedom have been examined in linear THz spectroscopy at low field levels but rarely if ever driven by strong ones. Furthermore, rather general capabilities for high-power THz waveform shaping encourage efforts going beyond THz coherent *spectroscopy of* to THz coherent *control over* the same array of collective and molecular responses.

Here, we briefly review our capabilities for generation, manipulation and control, and visualization of THz fields, collectively coined "THz polaritonics" [32], and our recent results in high-power THz generation using tilted pulse fronts as described earlier. We then present several results demonstrating nonlinear electronic and vibrational responses driven by the THz fields that we generate. We believe that the results presented here foreshadow far more ambitious prospects for THz coherent spectroscopy and control of material structure and dynamics.

II. Polaritonics Toolset

There are three primary components of the polaritonics toolset that distinguish it from more conventional THz and femtosecond optical methodology.

1) Spatiotemporal coherent control over polariton generation and propagation.
2) Spatiotemporal imaging of polariton fields and their evolution.
3) Integrated polaritonic functional elements including waveguides, resonators, and more complex elements composed of them.

Although the lateral propagation of THz polaritons poses challenges, it is precisely this attribute that enables the key polaritonics capabilities. Some of these are illustrated in Fig. 2. The use of additional light components beyond the first for THz wave imaging and manipulation is illustrated schematically in Fig. 2(a)–(c), which shows experimental results including polariton propagation in a waveguide structure. The illustration of polariton amplification in Fig. 2(b) is of particular interest. As suggested by the top view depicted in Fig. 1(c), successive, cylindrically focused optical pulses are shifted toward the right spatially and are delayed temporally such that the region of

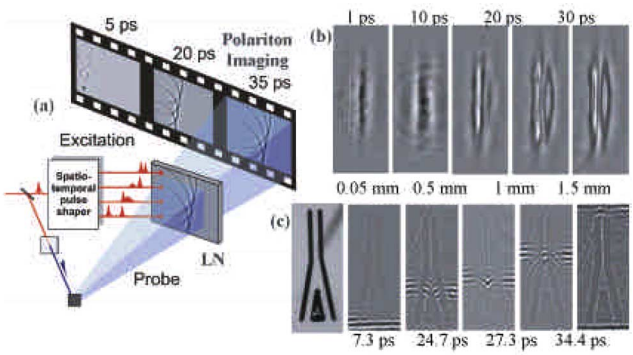

Fig. 2. Terahertz polaritonics: a solid-state platform for THz wave generation, control, guidance, processing, and visualization. (a) Schematic illustration. The components of a spatiotemporally "shaped" optical field arrive at different locations and times at the high-dielectric crystal to generate and manipulate a THz polariton response. Real-space imaging permits direct visualization of the propagating THz waves. (b) Polariton amplification. Images of a THz wave that is amplified by spatially and temporally shifted optical beams [as shown in the top view of Fig. 1(c) but with additional light beams only on the right-hand side of the first one and as viewed from the front of the crystal]. The delay times at which the images were recorded relative to the first excitation pulse arrival time are shown above the images, and the lateral shifts of the imaged regions of the crystal relative to the location of the first pulse are shown below. The polariton wave increases markedly in amplitude as it propagates across the crystal. (c) Polaritonic signal processing. Images of polariton waves entering a waveguide "Y-coupler" that has been integrated directly into an LN crystal through femtosecond laser fabrication. The coupler is illustrated in the micrograph at the left, in which the dark regions are air trenches that have been carved all the way through the crystal and the unmachined crystalline regions in between the air trenches act as waveguides. Several-cycle polariton waves enter the two input waveguide channels, propagate to the mixing region where they superpose in phase, and continue in a symmetric mode of the output waveguide channel. When the two incident THz waves are out of phase (not shown in the figure), they combine in an antisymmetric mode of the output waveguide channel.

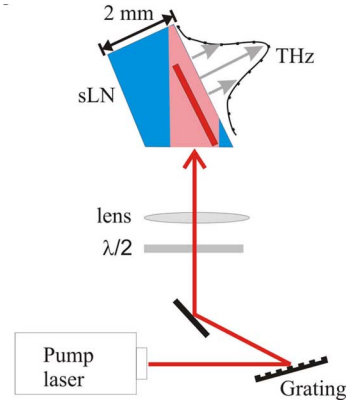

Fig. 3. Experimental setup for THz generation by tilted pulse front excitation. A grating generates a tilted optical pulse front and a lens adjusts the degree of tilt. The LN crystal is cut such that the amplified THz wave reaches the output face at normal incidence and is coupled out.

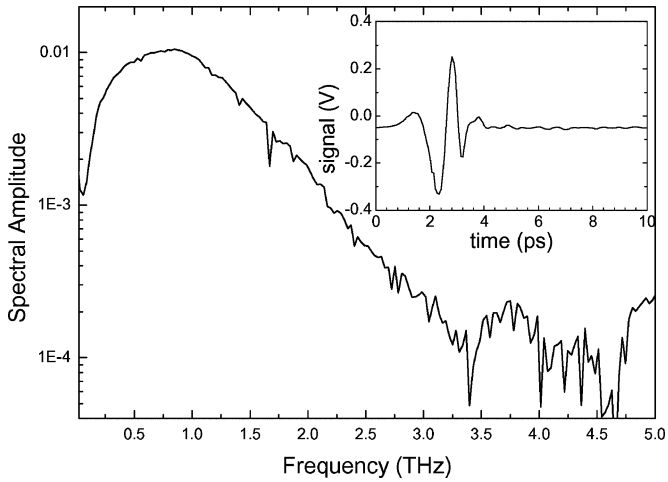

Fig. 4. Temporal profile and power spectrum of THz field generated as shown in Fig. 3. The profile indicates a nearly single-cycle pulse centered at around 0.8 THz frequency.

arrival moves rightward at a speed that matches the lateral phase velocity of the THz polariton wave. The successive optical field components generate additional THz field components that superpose with the original one to form a THz single-cycle wave whose amplitude grows to a far higher level than that generated by any one optical pulse whose intensity is below the crystal damage threshold. The result shown in Fig. 2(b) was achieved using an echelon (a stairstep glass structure) that splits an incident beam into several adjacent beams, with the pulses in adjacent beams delayed temporally by an amount that depends on the stairstep thickness [27]. A lens was used to adjust the spatial shift between adjacent beams at the LN crystal to match the lateral speed of the polaritons.

III. High-Power Polaritonics

As mentioned earlier, the simplest and most effective method for polariton amplification demonstrated till date uses only a grating and a lens to generate a continuous, tilted pulse front [28]–[30], see Fig. 3. This is superior to the discrete tilted pulse front used in the case of Fig. 2(b) because all of the crystalline volume can be used for polariton generation and amplification with no gaps between successive regions of the light field. Since polariton damping ultimately limits the amplification process, it is important to amplify throughout the polariton propagation region in order to most effectively compete with damping. Also shown in Fig. 3 is the bevel of the LN crystal such that the polariton wave reaches the output face at normal incidence. In this case, there is approximately 50% reflection and 50% transmission through the interface into free space. Single-cycle THz pulses were generated with more than 10 μJ of energy in this manner, a record amount for a tabletop system [33]. That result was achieved with an 800 nm pump laser system that produced about 20 mJ of optical pulse energy at a 10 Hz repetition rate.

Fig. 4 shows a typical temporal profile showing that a nearly single-cycle THz field is generated. The power spectrum of the pulse shows that its spectral content peaks at roughly 0.8 THz and extends to about 3 THz. In general, the polariton spectral content is limited by either the optical pulse duration or (more important in the present case) by the spatial width of the optical beam in the lateral direction, which directly determines the length of the THz polariton wave in its direction of propagation.

There is a good reason to anticipate that substantially greater THz pulse energies than the 10 μJ reported to date may soon

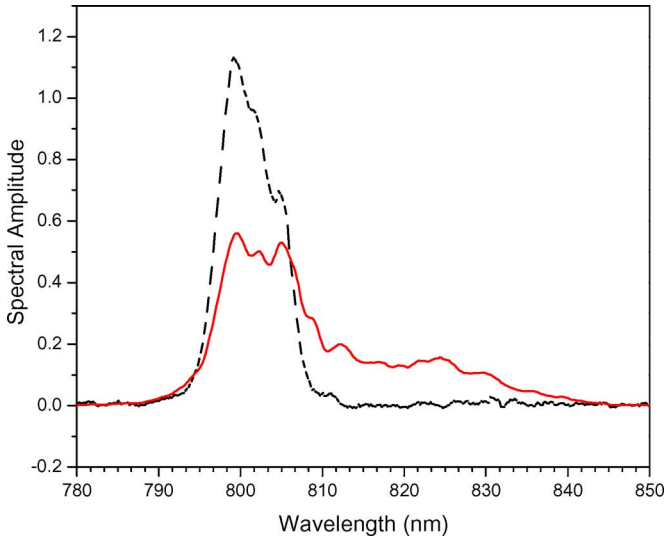

Fig. 5. Spectra of the optical pulse before (dashed curve) and after (solid curve) the LN crystal. The large redshift indicates high (∼800%) optical-to-THz photon conversion efficiency.

be reached with the same optical pulse energy. Fig. 5 shows the spectrum of the optical beam before and after passing through the LN crystal. A very substantial redshift of the pulse spectrum is evident. A simple calculation of the average wavelength (defined as the first moment) before and after the crystal showed an overall shift of just over 11 nm, or 5.3 THz, which when compared to the average THz frequency generated, 0.66 THz, indicates an overall optical-to-THz photon conversion efficiency of just over 800%. (There is no limit of 100% since THz generation occurs through difference-frequency mixing within the optical bandwidth, and this process can continue repeatedly [34] so that photons in the outgoing optical pulse, on average, have been shifted many times.) Calculation of the conversion efficiency based on 10 μJ THz pulse energy indicates about 45% photon conversion efficiency, and accounting for the 50% reflection at the output face yields an overall photon conversion efficiency of about 90%. The difference between this and the result suggested by the optical spectrum is presumably due to polariton damping, which can be reduced substantially by cooling of the LN crystal. This assumption is supported by the following estimation: the absorbed radiation can be obtained by integrating the product of efficiency based on [30, eq. (1)] and a 20 cm^{-1} linear absorption coefficient [35] for a 2-mm-long LN. The absorbed radiation thus calculated is 10 times larger than the measured THz output energy. The sum of the absorbed THz energy and the measured output energy yields the efficiency expected from the spectral change of the pump, when reflection losses are included. Nonlinear mechanisms may also be contributing to damping. These could include anharmonic vibrational decay channels that become active at large polariton amplitudes or polariton absorption by free carriers that are generated through multiphoton absorption of the optical pulse. Further work is under way to optimize conditions such that more of the THz response that is produced can be extracted.

Another approach to increased THz output has been described [27] and demonstrated on a preliminary basis. In polariton generation as illustrated in Fig. 1 or Fig. 3, the optical pump light is used once for the THz generation as it passes from front to back of the LN crystal. After that it plays no further role even though it still would be suitable for further THz generation. If an LN crystal with parallel front and back faces is used as depicted in Fig. 1, but the optical beam traverses the crystal at the complement of the Cherenkov angle instead of normal to the front and back surfaces, then one of the THz plane waves will propagate precisely laterally with respect to the front and back surfaces.

The light that is reflected by the back surface will be velocity matched with this THz response as it passes through the crystal for a second time. Referring to Fig. 1(b), the optical beam moves through the crystal along a path given by one of the grey lines and is reflected back through the crystal along a path given by the other grey line, the second traversal amplifying the THz response initiated by the first. This process could continue with subsequent reflections off the front and back faces, limited ultimately by polariton damping and dispersion. Using partial reflections off the faces of an uncoated crystal, a twofold enhancement of the polariton amplitude was measured, indicating a fourfold enhancement of the intensity. The optimization of this strategy, which can be applied with a tilted pulse front as well as a single beam, is under way.

While the highest THz pulse energies have been achieved at a 10 Hz repetition rate with ∼20 mJ of optical pulse energy, 3 mJ optical pulses at a 1 kHz repetition rate generated THz single-cycle pulses with ∼1 μJ energy [36]. This is sufficient to drive nonlinear responses in some materials, as illustrated later. In addition, splitting of the optical pulse into several collinear pulses through the use of parallel partial and high reflectors whose spatial separation could be varied (in the 100 μm range) to adjust the temporal spacing between the pulses yielded corresponding sequences of THz pulses with approximately the same total energy of 1 μJ. An example of a multiple-pulse THz waveform generated in this manner is shown in Fig. 6. More sophisticated approaches including temporal only and spatial only optical pulse shaping as well as spatiotemporal shaping [37]–[39], as illustrated in Fig. 2, have been used at lower power levels and will be entirely applicable at high power as well.

The results of tilted pulse front THz generation at higher repetition rates and with a 1.03 μm pump wavelength are also noteworthy. These outputs have not been used to drive nonlinear responses, but they have a wide range of potential applications including imaging, security screening, and signal processing. We summarize the results briefly here. With optical pulse energies in the 10–400 μJ range, the THz single-cycle pulse energies of 0.1–100 nJ were recorded. The THz pulse energy varied quadratically with the optical pulse energy throughout almost the entire range, until the latter exceeded 200 μJ. These THz output energies exceeded those we achieved from GaP (with collinear phase matching at this optical wavelength) and ZnTe (with a tilted pulse front at a far smaller tilt angle than in LN) by an order of magnitude or more. Measurement of the 400-μJ optical pulse spectrum before and after the LN crystal yielded a

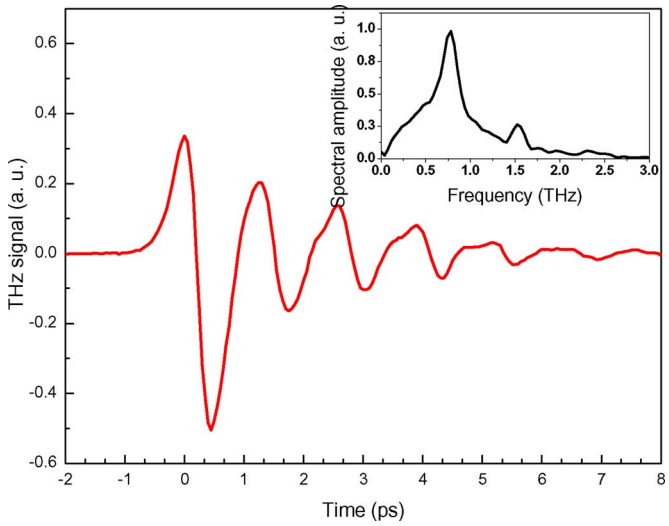

Fig. 6. THz multiple-cycle wave generated by a sequence of optical pulses. The spectrum is sharply peaked at the pulse repetition rate of 0.75 THz. A peak at the second harmonic frequency of 1.5 THz results from the fact that the optical pulse sequence did not have a purely sinusoidal form.

photon conversion efficiency of 90%, which was 11 times higher than that determined through measurement of the THz pulse energy and six times higher after taking the output face reflection into account. As discussed earlier, improved extraction of the THz energy that is generated may be possible under different pumping conditions. Finally, the 1.03 mm output of a fiber-based oscillator–amplifier system (Clark-MXR "Impulse") operating at a 1 MHz repetition rate and containing 10 W average power was used to generate approximately 1 mW THz average power (i.e., 1 nJ THz pulses). This result was achieved using an optical spot size that was better optimized for the 10 μJ optical pulse energy than the results mentioned earlier in which the same focusing conditions were used throughout the 10–400 μJ range.

The results overall demonstrate that the tilted pulse front approach to the THz generation is extremely effective over a very wide range of optical pulse energies that correspond to a wide range of repetition rates from about 10 Hz to 1 MHz. Throughout this range, the THz pulse energies achieved are to our knowledge the highest reported till date from a tabletop system of any kind. At the higher energies, their applicability to nonlinear spectroscopy and coherent control are strongly suggested.

One factor contributing to the good performance achieved is the higher figure of merit (FOM) value [30] of the LN compared to other electrooptic materials (see [30, Table I]). The other factor is that the LN is a dielectric with a large bandgap, contrary to the semiconductor electrooptic crystals that have smaller bandgaps. In these materials, generation of free carriers is possible by two-photon absorption, resulting in increased THz absorption. Only three-photon absorption is possible for 800 nm pumping in the LN, and only four-photon absorption for 1 μm pumping. Therefore, larger pump intensity can be used without significant free carrier generation.

Although the spectrum was restricted to the 0.1–3 THz range in the aforementioned cases, cooling the LN crystal [30] will enable efficient generation of up to 5 THz.

IV. THz Nonlinear Optics and Spectroscopy

Here, we offer several examples of nonlinear responses driven by high THz pulse energies and high THz field levels generated as described earlier. Nonlinear electronic responses induced by THz fields have been studied in a variety of semiconductors and in Rydberg atoms [4], [40]. The THz transition dipoles of some of these systems, in particular those associated with Rydberg transitions and with intersubband transitions in semiconductor nanostructures [41], are extremely large since the transitions involve the motion of a full electronic charge across a distance in the order of 1 nm (the approximate radius of a Rydberg atom or width of a quantum well structure). We have also observed nonlinear electronic responses in the form of induced absorption and emission in semiconductors. However, our emphasis here is on responses that involve a substantial ionic component. Thus, we have conducted initial measurements of nonlinearities in LN crystals, exploiting the same strongly polar soft vibrational mode that gives rise to the polaritons that we are generating. This provides a useful testbed for exploration of lattice-based nonlinearities. Although the LN at room temperature and below is deep in its ferroelectric phase, the fact that the material is ferroelectric and can be switched between two different domain orientations indicates significant anharmonicity associated with the double-well lattice potential and the barrier between the wells. First-principles calculations of LN and the closely related $LiTaO_3$ potential energy surface have been reported [42].

A. Lattice Anharmonicity 1—Dual-Beam THz Excitation and Direct Optical Observation

In an effort at direct observation of lattice anharmonicity in the LN, an experiment was performed in which two distinct THz fields were overlapped in an LN crystal, and the time-dependent response was measured optically [43]. The measurement made use of several of the polaritonics toolset components reviewed earlier. Although an echelon structure was used to produce distinct lines of light [as used to generate the response shown in Fig. 2(b)] rather than a grating to generate a continuous tilted pulse front, and a 1 kHz repetition rate system was used that delivered about 2 mJ total optical pulse energy to the LN crystal in which both the THz generation and the nonlinear measurements were carried out, nevertheless, the results clearly indicated an anharmonic lattice response. The experiment was executed as illustrated schematically in Fig. 7(a). An optical pulse was split by the echelon structure into about 20 vertical lines of light to form a discrete tilted pulse front that was imaged onto the surface of a 100-μm-thick LN crystal. A horizontal beam block was inserted into the optical path so that the top and bottom parts of the pulse front, but not the middle part, reached the sample. The top and bottom parts were chopped at two different frequencies f_1 and f_2. At the two irradiated horizontal regions of the LN crystal, polariton waves were generated and amplified. The amplified THz waves encountered a parabolic air trench that had been fabricated through femtosecond laser machining [as in Fig. 2(c)] and that acted as a focusing reflector. The two THz beams were focused and crossed at a region of the crystal that was not otherwise subjected to the THz irradiation. Although

polariton amplification was conducted in a manner similar to that illustrated in Fig. 2(b), the 100 μm LN crystal acts as a planar THz waveguide with multiple modes that have different phase and group velocities. As a result, rather than single-cycle THz waves, multiple-cycle waves at approximately 0.5 THz frequency were generated. The lattice response to these waves was monitored through measurement of transient birefringence, i.e., optical Kerr effect (OKE), signals with 400 nm probe pulses. The lattice response to each THz wave individually was measured at the separate chopping frequencies f_1 and f_2, and the nonlinear lattice response to both waves was detected at the sum or difference frequency $f_1 \pm f_2$. The results are shown in Fig. 7(c) and (d). The time-dependent nonlinear signal at the harmonic frequency of 1 THz is evident in the raw data and in the power spectrum. Fig. 7(b) shows the quadratic dependence of this signal component on the incident THz field amplitude. The largest amplitudes were estimated to be around 50 kV/cm. Amplitudes of nearly 1 MV/cm have been achieved with tilted pulse front THz generation using 20 mJ optical pulses at 10 Hz repetition rate.

We anticipate that substantially higher order lattice anharmonicity will be observed with larger fields. The use of more sophistocated THz waveform shaping may enable extensive coherent control over ferroelectrics and other materials with multiple stable or metastable configurations.

B. Lattice Anharmonicity 2—Polariton Harmonic Generation

The THz field amplitudes in the LN crystals used for THz generation by the tilted pulse front can be higher than those used for observation of the nonlinear lattice responses described earlier. Therefore, one might expect nonlinear responses to be apparent in the THz output. Fig. 8 shows that such responses can be observed. Fig. 8(a) shows a THz field profile recorded at 1 kHz repetition rate using pulses with about 2 mJ (solid) or just over 0.2 mJ (dashed). Fig. 8(b) shows the power spectra of the two profiles. When full power is used, the field profile shows additional time-dependent oscillations, and the power spectrum shows a progression of peaks and nulls. These features are not observed at low optical pulse energies. The spectral structure appears to reveal harmonics of the 0.75 THz peak frequency.

Because of the role of lattice anharmonicity in nonlinear responses at THz frequencies, the nonlinear coefficient d can be significantly larger [44] if both the fundamental and harmonic frequencies are below the transverse optic phonon frequency (the soft mode frequency in ferroelectric crystals) than at visible or near-IR frequencies. For the LN, $d = 30$ pm/V for the visible and $d = 5870$ pm/V in the THz range [44]. The standard expression for second harmonic generation efficiency [45] in a crystal with interaction length L (about 1 mm in the present case) and refractive indexes at fundamental and second harmonic frequencies n_{F} and n_{SH}, respectively.

$$\eta = \frac{2\omega^2 d^2 L^2}{\varepsilon_0 n_{\mathrm{F}}^2 n_{\mathrm{SH}} c^3} I_{\mathrm{F}} \tag{1}$$

indicates that we should expect a few percent conversion efficiency under our experimental conditions, in qualitative agreement with our observations. Note that these measurements were conducted at a 1 kHz repetition rate, not with our highest energy optical pulses, but due to tighter focusing into the LN crystal, to a region of approximately 1.5 mm $\times$ 2 mm, the intensity was somewhat higher than the level we typically reach at 1 kHz or 10 Hz. Focusing of the THz waves that we generate into

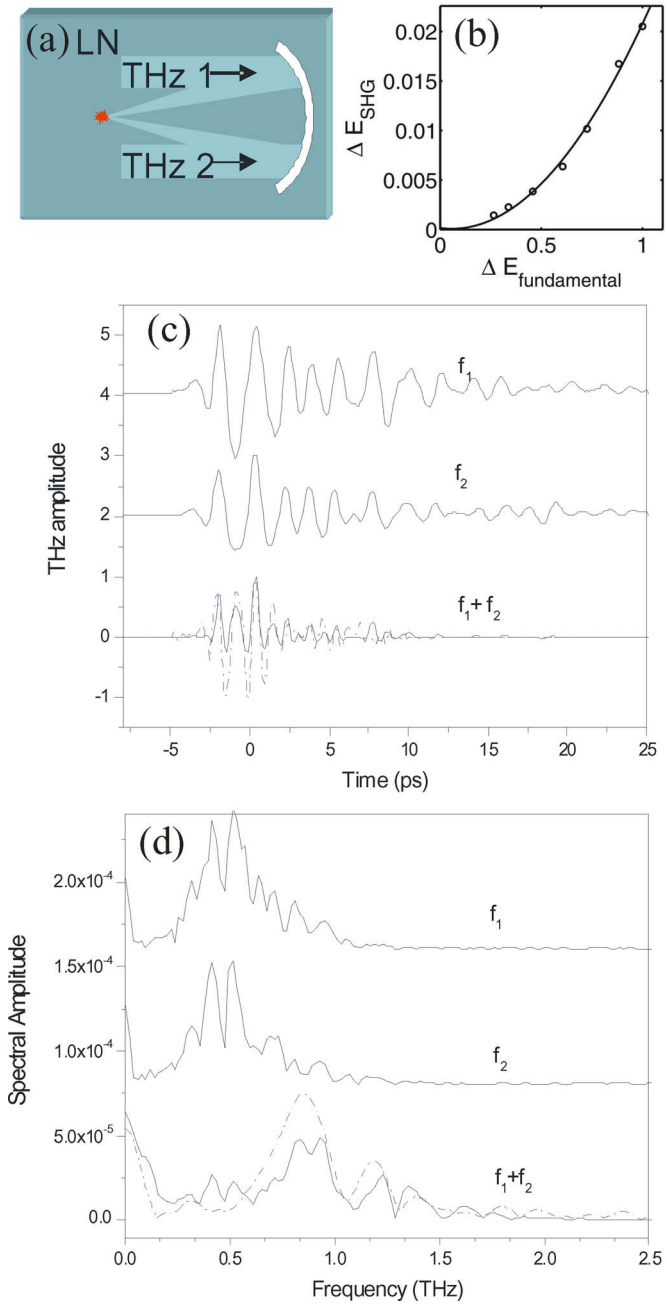

Fig. 7. Nonlinear THz spectroscopy of LN. (a) Schematic illustration. Two 0.5 THz waves are generated at different chopping frequencies f_1 and f_2, amplified, and directed to a common focus that is probed optically. Linear sample responses to each THz wave are monitored at the chopping frequencies, and nonlinear sample responses to both waves are detected at frequency $f_1 \pm f_2$. (b) Quadratic dependence of the harmonic signal on the fundamental 0.5 THz field amplitude. (c) Time-dependent OKE signal detected at the frequencies indicated. The bottom trace shows oscillations at the harmonic frequency of 1 THz. A fit to the data was generated from the incident 0.5 THz field assuming a quadratic nonlinearity in the sample response. (d) Power spectra of the traces in (c). The harmonic signal in the bottom trace is apparent.

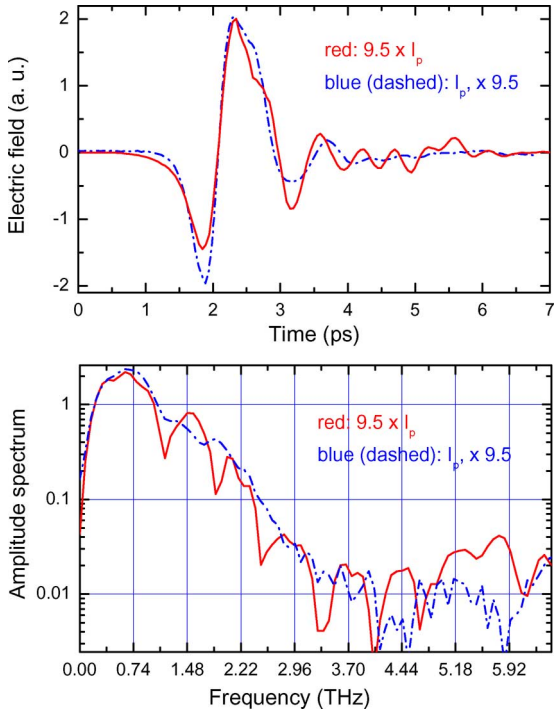

Fig. 8. Harmonic generation in the LN. (a) THz field profiles measured through electrooptic sampling with high and low optical and THz intensities. (The low intensity curve is multiplied by 9). (b) Amplitude spectra of field profiles in (a). At high power, peaks appear at harmonics of the 0.74 THz maximum frequency.

nonlinear crystals like the LN or $LiTaO_3$ (whose THz nonlinear coefficient exceeds that of LN by a factor of 3) should generate measurable harmonics from materials distinct from the THz generation crystals as well.

C. Lattice Anharmonicity 3—Self-Phase Modulation

Fig. 9 shows THz field profiles and power spectra from a LN crystal at 10 K that was pumped at a 1 kHz repetition rate with the full optical pulse energy (about 2 mJ) and with 1/3 of that amount. At high intensity, the THz field profile shows more oscillations than at low intensity, and there is clearly a change in the phase behavior of the oscillations. The origin of this effect is evident from the power spectra. At high intensity, the THz spectrum shows a dip at around the peak region ($\sim$ 0.8–1.4 THz) of the low-intensity spectrum and an increase at each of the wings of the low-intensity spectrum. The effect is revealed most clearly in the (dashed) plot of the ratio of the spectra. This behavior is typical of self-phase-modulation (SPM). Actually, the SPM is so strong in this case that it can be observed directly in the temporal profiles. For example, the delay between the first positive peak and the second negative peak is 200 fs larger at high intensity than at low intensity. This extra delay τ is caused by the THz-intensity-dependent change in the THz index of refraction, i.e., by the SPM. We can estimate the index change Δn according to

$$\Delta n = \frac{\tau c}{L} = n_2 I_{\mathrm{THz}} \tag{2}$$

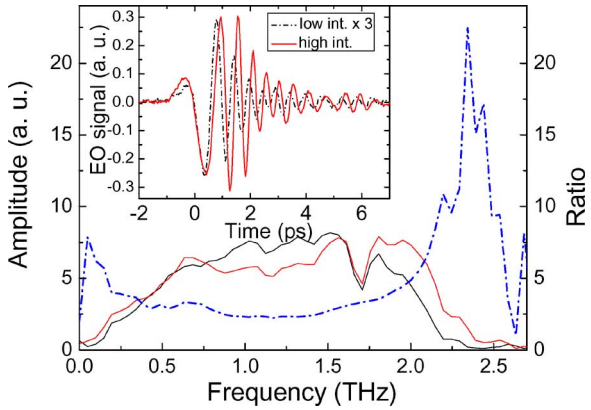

Fig. 9. Self-phase modulation in the LN. The temporal and spectral profiles of the THz fields at high and low intensities show clear differences. The ratio of high- to low-intensity spectra, plotted in blue (dashed), shows that at high intensity, the spectral amplitude is increased on both wings of the spectrum at the expense of the center, typical of the SPM.

with $L \approx 1$ mm as an approximate interaction length in the crystal. With this, we obtain $\Delta n = 0.06$. Using this value and the intensity $I_{\mathrm{THz}} \approx 1.3 \times 10^8$ W/cm^2 yield a nonlinear refractive index value $n_2 \approx 4.6 \times 10^{-10}$ cm^2/W at THz frequencies. By comparison, the value in the visible spectral range is $n_2 \approx 5.3 \times 10^{-15}$ cm^2/W [46]. This again emphasizes the very large role played by lattice anharmonicity in mediating nonlinear responses at THz frequencies.

V. Summary

Tabletop generation of THz pulses with energies of many microjoules and field levels in the order of 1 MV/cm at 1 THz frequency is now possible in a routine and reliable manner. An extensive toolset is available for shaping of the THz fields and for their manipulation and processing. These capabilities foreshadow broad applications in THz nonlinear optics, nonlinear spectroscopy, and coherent control. The area is at an early stage, but the prospects for spectroscopy and control over the motions of dipoles and ions as well as electrons are becoming clear. More ambitious prospects for control over collective material and electronic structure await realization.

References

[1] B. Ferguson and X.-C. Zhang, "Materials for terahertz science and technology," *Nature Mater.* vol. 1, pp. 26–33, 2002.
[2] C. A. Schmuttenmaer, "Exploring dynamics in the far-infrared with terahertz spectroscopy," *Chem. Rev.*, vol. 104, no. 4, pp. 1759–1780, 2004.
[3] Y. Shen, T. Watanabe, D. A. Arena, C.-C. Kao, J. B. Murphy, T. Y. Tsang, X. J. Wang, and G. L. Carr, "Nonlinear cross-phase modulation with intense single-cycle terahertz pulses," *Phys. Rev. Lett.*, vol. 99, pp. 043901-1–043901-4, 2007.
[4] R. R. Jones, D. You, and P. H. Bucksbaum, "Ionization of Rydberg atoms by subpicosecond half-cycle electromagnetic pulses," *Phys. Rev. Lett.*, vol. 70, pp. 1236–1239, 1993.
[5] T. Bartel, P. Gaal, K. Reimann, M. Woerner, and T. Elsaesser, "Generation of single-cycle THz transients with high electric-field amplitudes," *Opt. Lett.*, vol. 30, pp. 2805–2807, 2005.
[6] X. Xie, J. Dai, and X. C. Zhang, "Coherent control of THz wave generation in ambient air," *Phys. Rev. Lett.*, vol. 96, pp. 075005-1–075005-4, 2006.
[7] X. Xie, J. Xu, J. Dai, and X.-C. Zhang, "Enhancement of terahertz wave generation from laser induced plasma," *Appl. Phys. Lett.*, vol. 90, pp. 141104-1–141104-3, 2007.

[8] K.-Y. Kim, J. H. Glownia, A. J. Taylor, and G. Rodriguez, "Terahertz emission from ultrafast ionizing air in symmetry-broken laser fields," *Opt. Exp.*, vol. 15, pp. 4577–4584, 2007.
[9] B. B. Hu, X.-C. Zhang, D. H. Auston, and P. R. Smith, "Free-space radiation from electrooptic crystals," *Appl. Phys. Lett.*, vol. 56, pp. 506–508, 1990.
[10] K. Wynne and J. Carey, "An integrated description of terahertz generation through optical rectification, charge transfer, and current surge," *Opt. Commun.*, vol. 256, pp. 400–413, 2005.
[11] M. Schall and P. Uhd Jepsen, "Above-band-gap two-photon absorption and its influence on ultrafast carrier dynamics in ZnTe and CdTe," *Appl. Phys. Lett.*, vol. 80, pp. 4771–4773, 2002.
[12] M. C. Beard, G. M. Turner, and C. A. Schmuttenmaer, "Transient photoconductivity in GaAs as measured by time-resolved THz spectroscopy," *Phys. Rev. B.*, vol. 62, pp. 15764–24777, 2000.
[13] A. Nahata, A. S. Weling, and T. F. Heinz, "A wideband coherent terahertz spectroscopy system using optical rectification and electro-optic sampling," *Appl. Phys. Lett.*, vol. 69, pp. 2321–2323, 1996.
[14] F. Blanchard, L. Razzari, H. C. Bandulet, G. Sharma, R. Morandotti, J. C. Kieffer, T. Ozaki, M. Reid, H. F. Tiedje, H. K. Haugen, and F. A. Hegmann, "Generation of 1.5 μJ single-cycle terahertz pulses by optical rectification from a large aperture ZnTe crystal," *Opt. Exp.*, vol. 15, pp. 13212–13220, 2007.
[15] T. Löffler, T. Hahn, M. Thomson, F. Jacob, and H. Roskos, "Large-area electro-optic ZnTe terahertz emitters," *Opt. Exp.*, vol. 13, pp. 5353–5362, 2005.
[16] G. Chang, C. J. Divin, C.-H. Liu, S. L. Williamson, A. Galvanauskas, and T. B. Norris, "Power scalable compact THz system based on an ultrafast Yb-doped fiber amplifier," *Opt. Exp.*, vol. 14, pp. 7909–7913, 2006.
[17] A. S. Barker and R. Loudon, "Response functions in the theory of Raman scattering by vibrational and polariton modes in dielectric crystals," *Rev. Mod. Phys.*, vol. 44, pp. 18–47, 1972.
[18] T. P. Dougherty, G. P. Wiederrecht, and K. A. Nelson, "Impulsive stimulated Raman scattering experiments in the polariton regime," *J. Opt. Soc. Amer. B.*, vol. 9, pp. 2179–2189, 1992.
[19] D. H. Auston, K. P. Cheung, J. A. Valdmanis, and D. A. Kleinman, "Cherenkov radiation from femtosecond optical pulses in electro-optic media," *Phys. Rev. Lett.*, vol. 53, pp. 1555–1558, 1984.
[20] A. G. Stepanov, J. Hebling, and J. Kuhl, "THz generation via optical rectification with ultrashort laser pulse focused to a line," *Appl. Phys. B*, vol. 81, pp. 23–26, 2005.
[21] A. G. Stepanov, J. Hebling, and J. Kuhl, "Generation, tuning, and shaping of narrow-band, picosecond THz pulses by two-beam excitation," *Opt. Exp.*, vol. 12, pp. 4650–4658, 2004.
[22] R. M. Koehl, S. Adachi, and K. A. Nelson, "Direct visualization of collective wavepacket dynamics," *J. Phys. Chem. A*, vol. 103, pp. 10260–10267, 1999.
[23] R. M. Koehl, S. Adachi, and K. A. Nelson, "Real-space polariton wave packet imaging," *J. Chem. Phys.*, vol. 110, pp. 1317–1320, 1999.
[24] T. Feurer, J. C. Vaughan, and K. A. Nelson, "Spatiotemporal coherent control of lattice vibrational waves," *Science*, vol. 299, pp. 374–377, 2003.
[25] R. M. Koehl and K. A. Nelson, "Coherent optical control over collective vibrations traveling at light-like speeds," *J. Chem. Phys.*, vol. 114, pp. 1443–1446, 2001.
[26] R. M. Koehl and K. A. Nelson, "Terahertz polaritonics: Automated spatiotemporal control over propagating lattice waves," *Chem. Phys.*, vol. 267, pp. 151–159, 2001.
[27] K.-L. Yeh, T. Hornung, J. C. Vaughan, and K. A. Nelson, "THz amplification in high-dielectric materials," in *Ultrafast Phenomena XV*, P. Corkum, D. Jonas, R. J. D. Miller, and A. M. Weiner, Eds. New York: Springer-Verlag, 2007, pp. 802–804.
[28] J. Hebling, G. Almasi, I. Kozma, and J. Kuhl, "Velocity matching by pulse front tilting for large area THz-pulse generation," *Opt. Exp.*, vol. 10, pp. 1161–1166, 2002.
[29] A. G. Stepanov, J. Hebling, and J. Kuhl, "Efficient generation of subpicosecond terahertz radiation by phase-matched optical rectification using ultrashort laser pulses with tilted pulse fronts," *Appl. Phys. Lett.*, vol. 83, pp. 3000–3002, 2003.
[30] J. Hebling, A. G. Stepanov, G. Almási, B. Bartal, and J. Kuhl, "Tunable THz pulse generation by optical rectification of ultrashort laser pulses with tilted pulse fronts," *Appl. Phys. B*, vol. 78, pp. 593–599, 2004.
[31] A. G. Stepanov, J. Kuhl, I. Z. Kozma, E. Riedle, G. Almási, and J. Hebling, "Scaling up the energy of THz pulses created by optical rectification," *Opt. Exp.*, vol. 13, pp. 5762–5768, 2005.
[32] T. Feurer, N. S. Stoyanov, D. W. Ward, J. C. Vaughan, E. R. Statz, and K. A. Nelson, "Terahertz polaritonics," *Annu. Rev. Mater. Res.*, vol. 37, pp. 317–350, 2007.
[33] K.-L. Yeh, M. C. Hoffmann, J. Hebling, and K. A. Nelson, "Generation of 10 μJ ultrashort THz pulses by optical rectification," *Appl. Phys. Lett.*, vol. 90, pp. 171121-1–171121-3, 2007.
[34] M. Cronin-Golomb, "Cascaded nonlinear difference-frequency generation of enhanced terahertz wave production," *Opt. Lett.*, vol. 28, pp. 2046–2048, 2004.
[35] L. Pálfalvi, J. Hebling, J. Kuhl, Á. Péter, and K. Polgár, "Temperature dependence of the absorption and refraction of Mg-doped congruent and stoichiometric $LiNbO_3$ in the THz range," *J. Appl. Phys.*, vol. 97, pp. 123505-1–123505-6, 2005.
[36] K.-L. Yeh, J. Hebling, M. C. Hoffmann, and K. A. Nelson, submitted for publication.
[37] N. S. Stoyanov, D. W. Ward, T. Feurer, and K. A. Nelson, "Terahertz polariton propagation in patterned materials," *Nature Mater*, vol. 1, pp. 95–98, 2002.
[38] G. P. Wiederrecht, T. P. Dougherty, L. Dhar, and K. A. Nelson, "Explanation of anomalous polariton dynamics in $LiTaO_3$," *Phys. Rev. B*, vol. 51, pp. 916–931, 1995.
[39] T. Feurer, J. Vaughan, T. Hornung, and K. A. Nelson, "Typesetting of THz waveforms," *Opt. Lett.*, vol. 29, pp. 1802–1804, 2004.
[40] P. Gaal, K. Reimann, M. Woerner, T. Elsaesser, R. Hey, and K. H. Ploog, "Nonlinear terahertz response of n-type GaAs," *Phys. Rev. Lett.*, vol. 96, pp. 187402-1–187402-4, 2006.
[41] S. G. Carter, V. Birkedal, C. S. Wang, L. A. Coldren, A. V. Maslov, D. S. Citrin, and M. S. Sherwin, "Quantum coherence in an optical modulator," *Science*, vol. 310, pp. 651–653, 2005.
[42] I. Inbar and R. E. Cohen, "Comparison of the electronic structures and energetics of ferroelectric $LiNbO_3$ and $LiTaO_3$," *Phys. Rev. B*, vol. 53, pp. 1193–1204, 1996.
[43] T. Hornung, K.-L. Yeh, and K. A. Nelson, "Terahertz nonlinear response in lithium niobate," in *Ultrafast Phenomena XV*, P. Corkum, D. Jonas, R. J. D. Miller, and A. M. Weiner, Eds. New York: Springer-Verlag, 2007, pp. 772–774.
[44] G. D. Boyd and M. A. Pollack, "Microwave nonlinearities in anisotropic dielectrics and their relation to optical and electro-optical nonlinearities," *Phys. Rev. B*, vol. 7, pp. 5345–5459, 1973.
[45] R. L. Sutherland, *Handbook of Nonlinear Optics*. New York: Marcel Dekker, 1996.
[46] L. Heping, Z. Feng, Z. Xejung, and J. Wei, "Picosecond Z-scan study of bound electronic Kerr effect in $LiNbO_3$ crystal associated with two-photon absorption," *Appl. Phys. B*, vol. 64, pp. 659–662, 1997.

János Hebling received the M.S. and Ph.D. degrees in physics from the József Attila (JATE) University, Szeged, Hungary, in 1978 and 1982, respectively.

He was with the JATE University. He was with the Max-Planck Institute for Solid State Research, Stuttgart, Germany, for more than six years. Since 1999, he has been the Head of the Experimental Physics Department, University of Pécs, Pécs, Hungary. He is a Doctor of the Hungarian Academy of Sciences. He is currently at Massachusetts Institute of Technology, Cambridge. His current research interests include ultrafast time-resolved spectroscopy of solids, nonlinear optics, and terahertz pulse generation.

Dr. Hebling is the recipient of the Pál Selényi Award.

Ka-Lo Yeh received the B.Sc(Hons.) in chemistry and computational science from the National University of Singapore, Singapore, in 2003.

She is currently a fifth year graduate Research Assistant in the Keith Nelson Group, Department of Chemistry, Massachusetts Institute of Technology, Cambridge.

Matthias C. Hoffmann received the Ph.D. degree in physics from the University of Freiburg, Freiburg, Germany, in 2006.

He is currently a Postdoctoral Fellow at Massachusetts Institute of Technology, Cambridge. His current research interests include terahertz (THz) spectroscopy of solids with intense single-cycle pulses.

Keith A. Nelson received the B.S. and Ph.D. degrees in chemistry and physical chemistry Stanford University, Stanford, CA, in 1976 and 1981, respectively.

He was a Postdoctoral Scholar at the University of California, Los Angeles (UCLA). In 1982, he joined the Department of Chemistry, Massachusetts Institute of Technology (MIT), Cambridge. His current research interests include ultrafast spectroscopy of condensed phase structural and chemical rearrangements and the collective degrees of freedom that mediate them, the development of terahertz and optical pulse shaping methods that enable coherent control over collective modes including acoustic phonons, optic phonons, phonon–polaritons, and excitons.